NANO LETTERS

2007
Vol. 7, No. 4
1076−1080

Nanopin Plasmonic Resonator Array and Its Optical Properties

Sheng Wang, David F. P. Pile, Cheng Sun, and Xiang Zhang*

National Science Foundation Nanoscale Science and Engineering Center (NSEC), 5130 Etcheverry Hall, University of California, Berkeley, California 94720-1740

Received December 11, 2006; Revised Manuscript Received February 21, 2007

ABSTRACT

A one-step electron-beam lithography process for the fabrication of a high-aspect ratio nanopin array is presented. Each nanopin is a metal-capped dielectric pillar upon a ring-shaped metallic disc. Highly tunable optical properties and the electromagnetic interplay between the metallic components were studied by experiment and simulation. The two metallic pieces play asymmetrical roles in their coupling to each other due to their drastic size difference. The structure can lead to ultrasensitive surface-enhanced Raman scattering chemical sensor arrays, etc.

Resonant excitation of localized surface plasmons in metallic nanostructures is one of the major approaches for concentrating and enhancing electromagnetic energy on the nanoscale.[1−4] It offers unique opportunities for the development of near-field optical microscopy with subwavelength resolution,[5−9] high-resolution lithography,[10] coupling of light into and out of photonic nanocircuits,[1−3,11−14] etc. One of the most important applications of localized surface plasmons is new sensors based on surface-enhanced Raman scattering (SERS)[15−19] for detection of chemical, organic and biological compounds, thin films and interfaces, crystalline structures and defects, etc.

One common approach for achieving SERS is to use aggregated colloidal metallic (silver or gold) nanoparticles. So-called "hot-spots" at the narrow gaps between particles result in an enhancement of the local electric field, E, near the particle, leading to a strong ($\propto E^4$) SERS signal. The enhancement factor of these hot spots can reach 10^{14}.[16,19] However, there are significant disadvantages associated with this technique. The substance to be tested must be dissolved in the colloid. Reproducibility and efficiency are also major issues due to the stochastic nature of nanoparticle aggregation (hot-spots have a relatively low probability of occurring by random aggregation). Despite the ability to detect a single molecule near a hot-spot, the sample's amount should still be relatively large to produce a noticeable concentration in the colloid. Therefore, various different plasmonic structures for reproducibly enhancing electromagnetic fields have been suggested. These include sharp metal tips,[1,20,21] dielectric conical tips covered in metal film,[5,7−9] nanoparticle lenses,[22] sharp metallic grooves and nanowedges,[2,13,14,23] plasmon interference,[24] nanoburgers,[25] etc. However, many of these techniques currently suffer from several challenging hurdles. For example, the focusing of plasmons in tapered plasmonic waveguides[1,2,13,14,20,23] has not been experimentally demonstrated to date due to challenges in fabrication and detection.

In this paper, we present a 3-piece "nanopin" array for reproducible and tunable plasmonic resonance. The entire array of high-aspect ratio nanopins is fabricated by a simple one-step electron-beam lithography process. Each nanopin is constituted by a metal-capped dielectric pillar sitting on a ring-shaped metallic disc. The one-step fabrication process, big effective volume with relatively large field enhancement, and high potential for tuning of the nanopin array are expected to be fruitful for the development of high-throughput SERS biosensor array, etc.

The fabrication flow is depicted in Figure 1. At first, 150 nm of poly(methyl methacrylate) (PMMA) was spin-coated onto the substrate (30 nm indium tin oxide (ITO) layer on a quartz wafer), shown in Figure 1a. Then the sample was exposed to an electron beam (quanta 200 HV from FEI company) but instead of the normal spot dose (∼100 to ∼1000 fC) we applied 40 000 fC (Figure 1b). The PMMA that receives the highest dose at the beam's center will be extensively cross-linked due to the electron-beam-induced radical reactions. This results in significantly increased molecular weight in that region. However, the PMMA exposed to the edge of the electron beam will receive a much lower dose. Therefore, after the development the center will extrude out but the surrounding will be etched (Figure 1c). Subsequently, we evaporated 20 nm of gold onto the sample (Figure 1d) and carried out the lift-off processes to transfer the pattern. Once again, because the center (with respect to the electron-beam spot) region of PMMA has higher molecular weight, it better endures the acetone. Thus, it can survive the short time duration of the lift-off process,

* Corresponding author. E-mail: xiang@berkeley.edu.

10.1021/nl062911y CCC: $37.00
Published on Web 03/08/2007

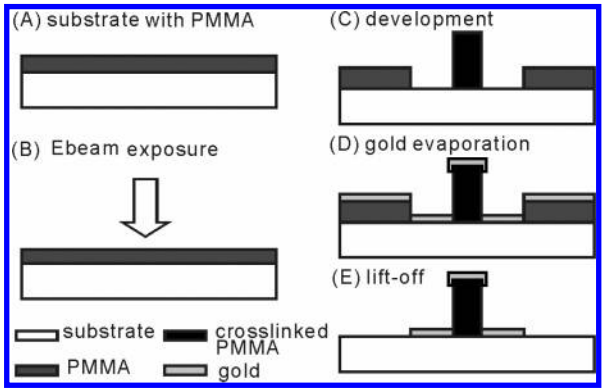

Figure 1. Schematic showing the fabrication flow of the nanopin array.

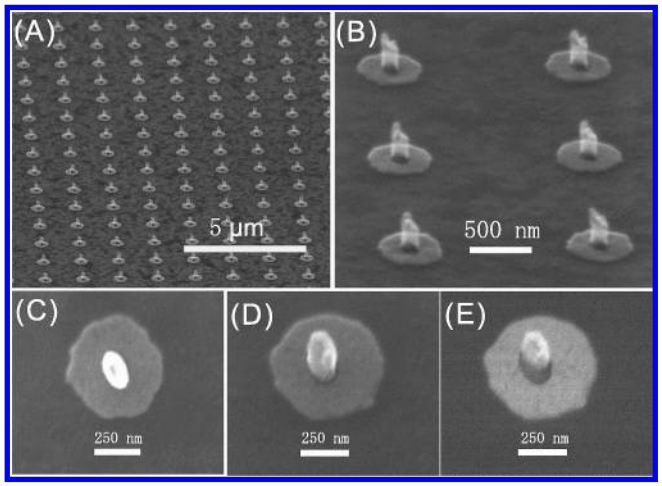

Figure 2. (A) SEM image of the nanopin structure array. (B) The zoomed-in image of (A). (C) The SEM top view of one "nanopin" structures. (D) The secondary electron image of one nanopin. (E) The backscattering electron image of the same structure as (D) (60° tilt-angle for (A) and (B); 20° tilt-angle for (D) and (E)).

and we finally obtain the three-dimensional (3D) array high-aspect ratio nanopin structure, which is schematically shown as Figure 1e. The radial sizes of the cap and bottom ring, which are associated due to the Gaussian distribution of the beam intensity, are adjustable by varying the exposure dose. The distance between top and bottom pieces is mainly proportional to the spin-coated PMMA thickness. Because the spot dose has to be high enough to enable the center cross-linked PMMA to survive during the lift-off processes, the typical size nanopin that can be robustly repeated in fabrication is the one we present in this letter. Further improvement in reducing the size is possible by optimizing the properties of PMMA, such as molecule weight or the spin-on thickness.

The nanopin structure was characterized and confirmed by scanning electron microscope (SEM) as shown in Figure 2. Figure 2a shows the array using a 60° tilt-angle. Individual nanopins are confirmed to be 1.5 μm apart from each other (as were designed), and we can see the structures exhibit excellent uniformity and repeatability (as long as the exposure doses are uniform and repeatable). Figure 2b is the zoomed-in image (with the same tilt-angle as Figure 2a), which better shows the 3D structure of the "pin". It reveals the center "pillar" that is around 300 nm tall. Figure 2c, which is the top view of an individual nanopin, indicates that the center pillar is actually elliptical in its cross-section. The short axis of the ellipse is ≈100 nm, and the long axis is ≈150 nm. The outer diameter of the bottom metal piece (ring-shaped disc) is ≈500 nm. To get additional information, we compared a conventional SEM secondary electron image (Figure 2d) to a backscattering electron image (Figure 2e), both with a tilt-angle of 20° (for a reliable backscattering electron image). According to the conventional SEM image (Figure 2d), it is unclear if the metallic film extends from the bottom disc up the side of the pillar and connects with the metallic cap on top of the pillar. However, we can see in the backscattering electron image (Figure 2e) that there is a dark region between the top and bottom metallic pieces that does not show up clearly in the secondary electron image (Figure 2d). Because the backscattering electron imaging is more sensitive to the element, we conclude that the gold is separated into two pieces (top and bottom) instead of a continuous film and that the structure is indeed that of the nanopin as the schematically shown structure in Figure 1e. At the same time, Figure 2e shows there is some gold extending from the top of the PMMA pillar and partly down the side wall (i.e., the resulting top metallic piece resembles a metallic "cap" as depicted schematically in Figure 1e). Possible causes for the extension of the metal down the side of the pillar can be the variation of the diameter of the PMMA pillar between its top and bottom or the evaporative edge effects due to the variation of evaporation direction. The extension of the cap down to the side of the pillar is estimated to be several tens of nanometers, but the accurate determination is nontrivial. In the later numerical simulations, we took the extension to be 30 nm (this is a reasonable value from our experience with evaporative edge effects).

As has been confirmed, the nanopin structure consists of two separate metallic pieces: a top small cap and the relatively larger bottom ring, each possessing its own individual optical responses and resonances. At the same time, if the two metallic pieces are sufficiently close together, the new hybridized mode will be formed due to their interactions.[26] To investigate such optical features, we experimentally measured the scattering spectrum of the nanopin structure and also conducted numerical simulations that elucidated the underlying physics of the experimentally obtained scattering spectrum.

We employed the total internal reflection (TIR) excitation geometry for the spectrum measurement; the principle of the TIR is schematically shown as Figure 3a. In our experiments, a collimated 150 W Xe white light source was incident (by a multimode optical fiber) normal to one surface of a right-angle prism and totally internally reflected. The nanopin array sat on the prism surface (at which total internal reflection occurred) in the evanescent field that penetrated from the prism and decayed into the surrounding media. Index-matching oil was used to minimize stray-scattering light due to surface defects, etc. The light scattered by the nanopins was collected by an optical microscope with a 50× long working distance objective (0.5 N.A.) and formed an image

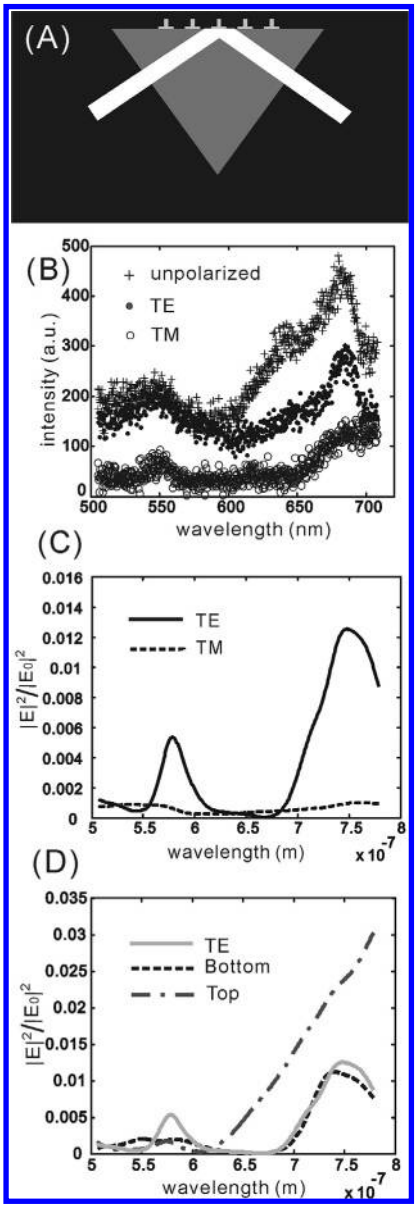

Figure 3. (A) The TIR configuration for the spectrum measurement experiment. (B) The experimentally obtained spectrum (including unpolarized (crosses), TE- (solid dots) and TM-polarized incident light (circles)). (C) The numerically obtained spectrum (TE- (solid curve) and TM- (dashed) polarized incident light). (D) The "control" simulation spectrum for TE-polarized incident light (including the whole structure (solid), only top piece (dash-dot) or only bottom piece (dashed)).

at the exit image plane. Between the scattering structure and the spectrometer (Triax Jobin Yvon type equipped with a liquid nitrogen-cooled charge-coupled device detector), we put a small aperture (~1 μm diameter) at the image plane to select a single nanopin. The measured spectrum is consistent (within the range of the experimental uncertainty) from that of different individual nanopins in the same array due to the reliable top-down fabrication method. Therefore, Figure 3b is the typical spectrum information for an individual-selected nanopin.

There are two maxima in the scattering spectrum for transverse-electric (TE)-polarized incident light, one at 550 nm and one just below 700 nm (solid dots in Figure 3b). For transverse-magnetic (TM)-polarized incident light, there are maxima of relatively (compared to TE polarization) weaker amplitude at the similar wavelengths (circles in Figure 3b). To clarify the origin spectral characteristics, we conducted numerical simulations employing a 3D finite-difference time-domain solution to the Maxwell equations (using Microwave Studio from CST company). The structural configuration we used for the computations are 20 nm thickness gold layer, bottom ring diameter of 500 nm, top particle diameter of 120 nm diameter (to make the model simple, we used a circular cross-sectioned particle instead of the real elliptical case), and 10 nm thickness gold extending 30 nm from the top disc down the PMMA pillar's sides. In the computation, the permittivity of the gold was represented by the Drude model, $\epsilon_{Au} = \epsilon_\infty - \omega_p^2/[\omega(\omega - i\gamma)]$, fitted to the experimental data[27] by using the Drude model parameters: $\epsilon_\infty = 10$, $\omega_p = 1.4e16$ rad/s, $\gamma = 1.1$ e 14 Hz (note that we assumed an effective-surrounding medium (representing the ITO and air) with dielectric permittivity 1.5). The scattered far-field light intensity was recorded 1 μm above the structure and the resultant simulated-scattering spectrum results are shown in Figure 3c. Similar maxima exist for the TE-polarized incident light and likewise, but again with weaker amplitude of the maxima for the TM-polarized incident light. Compared to the experimental spectrum, the maxima are 30−50 nm red-shifted. Some quantitative variations between the experimental results and numerical results are expected because the numerical structure does not precisely represent the real structure (e.g., possible differences may include metal and dielectric permittivities, the pillar shape, the thickness of the gold-coated on the PMMA pillar, etc).

To reveal the underlying physics of the nanopin-scattering spectrum we also calculated "control" simulation results for TE-polarized incident light (Figure 3d). The light solid curve is the spectrum of the total structure, while the dot-dash curve represents only the top cap's spectrum, and the dashed curve represents only the bottom ring's spectrum. Both pieces, bottom ring and top cap, exhibit a small maximum in the scattering spectrum at a relatively short wavelength. The overall scattering spectrum in this wavelength region is roughly the simple algebraic sum of that of the top and bottom pieces. Interestingly, as the wavelength passes 600 nm the overall structure spectrum is no longer the sum of the individual piece's spectra. Instead, it mainly resembles that of the bottom ring structure but with a slightly red-shifted peak position. The physical reason can be understood as follows. The two metallic pieces are ~300 nm apart and they are too far apart to interact strongly at short wavelengths (<600 nm). The two localized plasmons establish their own fields and form their resonance independently, which results in the overall spectrum being approximately the sum of those of the individual pieces. However, the localized field distribution at each metallic piece scales with the wavelength (i.e., the distance between the pieces is relatively shorter at a longer wavelength). Thus, increasing the wavelength eventually results in the field localized at one metallic piece having significant amplitude in the region of the adjacent

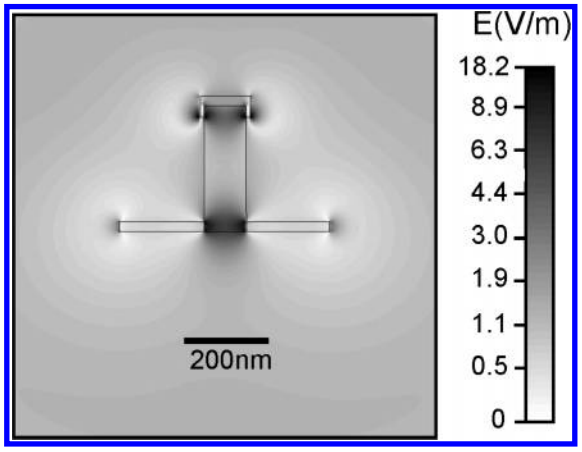

Figure 4. The electric field distribution in the cross-section for the entire nanopin structure at the resonance peak around 750 nm (the computational window is one micron cubed) determined by 3D finite-different time-domain solution to the Maxwell equations.

metallic piece (i.e., the particles begin to "feel" each other). This results in formation of new hybridized modes and drastic modification of the optical response of the combined structure compared to the sum of the optical responses of the single metallic pieces. However, as the two pieces interact (in the considered frequency range) the symmetrically coupled (bonding) plasmon mode, which carries the majority of energy of the two pieces' hybrization modes, will have a similar resonance peak to the big bottom piece's intrinsic spectrum but with a slightly red-shift due to the drastic size and energy difference between the two pieces, which agrees very well with our simulation curves (Figure 3d).[26]

Figure 4 is the numerically obtained electrical field amplitude, $|E|$, distribution around the whole structure at the resonant wavelength ($\approx$750 nm). The maximum field enhancement is 18.2 (331.2) times the incident light amplitude (intensity); the field is strongest near the ring and cap edges. Figure 4 also shows a large volume with a relatively large field enhancement. This is because of the big cross-section of the bottom piece that can receive the energy and redistribute it via the field through interactions between the top cap and the bottom ring. It is particularly relevant for designing a big effective volume SERS sensor because it cannot be easily confirmed if the sharp edges really exist in the fabricated structure. The considered wavelength is not yet at the resonance of the top piece (see Figure 3d), and there is therefore room for further optimization of parameters for obtaining stronger field enhancement. In particular, it should be possible and most interesting to engineer the structure so that the bottom and top pieces have more closely coinciding resonant wavelengths. In this case, the two localized modes can resonantly exchange electromagnetic energy, resulting in the formation of a new resonant-coupled mode of the entire nanopin that can be expected to have interesting optical characteristics including high sensitivity to structural and wave parameters (tunability) and the possibility of significantly stronger electromagnetic field enhancement. One of the great advantages of the presented fabrication process is the ease of modifying various structural parameters including the distance between the top and bottom pieces (by preparing different PMMA thickness), the cap and ring diameters (by varying the electron-beam exposure doses), etc. However, such optimization will require extensive analysis that is out of the scope of the present letter. Moreover, by taking advantages of top-down fabrication methods, the distance between nanopins can be easily varied by design that will provide another opportunity to tune the resonance frequency of the system.

In conclusion, we presented a simple one-step electron-beam lithography process to fabricate a high-aspect ratio nanopin array structure. Each nanopin is constituted by a metal-capped dielectric pillar sitting on a ring-shaped metallic disc. Although the structure is 3D, no alignment is needed. At the same time, we can make very uniform arrays or complex patterns, such as the nanopin array, and have the ability to easily select the desired distance between the individual structures and the diameter of the metal cap, dielectric pillar, and bottom ring by taking advantage of the top-down electron-beam lithography method. The nanopin's optical properties, including the scattering spectrum, resonant frequency, enhancement of the electromagnetic field, and the interactions between the two pieces, were studied by experiment and simulation. Physical reasons for the response of the system based on the experimental and numerical results were provided. We numerically predicted and experimentally observed that if the two metallic pieces were sufficiently close together (compared to the incident wavelength), the optical response was drastically modified. The two metallic pieces played asymmetrical roles in their coupling to each other due to their drastic size and energy difference. The possibility of structural improvements (and tuning) of the optical response and also significantly increasing the field enhancement were discussed. The one-step fabrication process, unique optical properties, and high potential for tuning and further improvement of the nanopin array are expected to be fruitful for the development of high-throughput ultrasensitive SERS chemical sensor arrays, etc.

Acknowledgment. This work was supported in part by NSF grant DMI-0455698, DMI-0427679, and NSF Nanoscale Science and Engineering Center (NSEC) (DMI−0327077), and the U.S. Air Force Office of Scientific Research MURI program under Grant No. FA9550-04-1-0434. We thank Werayut Srituravanich, Yi Xiong, Junyu Mai, and Zhaowei Liu for helpful discussions.

References

(1) Stockman, M. I. *Phys. Rev. Lett.* **2004**, *93*, 137404.
(2) Pile, D. F. P.; Gramotnev, D. K. *Appl. Phys. Lett.* **2006**, *89*, 041111.
(3) Bozhevolnyi, S. I.; Volkov, V. S.; Devaux, E.; Laluet, J.-Y.; Ebbesen, T. W. *Nature* **2006**, *440*, 508−511.
(4) Sundaramurthy, A.; Crozier, K. B.; Kino, G. S.; Fromm, D. P.; Schuck, P. J.; Moerner, W. E. *Phys. Rev. B* **2005**, *72*, 165409.
(5) Novotny, L.; Pohl, D. W.; Hecht, B. *Ultramicroscopy* **1995**, *61*, 1.
(6) Linden, S.; Rau, N.; Neuberth, U.; Naber, A.; Wegener, M.; Pereira, S.; Busch, K.; Christ, A.; Kuhl, J. *Phys. Rev. B* **2005**, *71*, 245119.
(7) Bouhelier, A.; Renger, J.; Beversluis, M. R.; Novotny, L. *J. Microsc.* **2003**, *210*, 220.
(8) Nerkararyan, K. V.; Abrahamyan, T.; Janunts, E.; Khachatryan, R.; Harutyunyan, S. *Phys. Lett. A* **2006**, *350*, 147.

(9) Mehtani, D.; Lee, N.; Hartschuh, R. D.; Kisliuk, A.; Foster, M. D.; Sokolov, A. P.; Cajko, F.; Tsukerman, I. *J. Opt. A* **2006**, *8*, S183.
(10) Srituravanich, W.; Fang, N.; Sun, C.; Luo, Qi.; Zhang, X. *Nano Lett.* **2004**, *4*, 1085.
(11) Maier, S. A.; Brongersma, M. L.; Kik, P. G.; Meltzer, S.; Requicha, A. A. G.; Atwater, H. A. *Adv. Mater.* **2001**, *13*, 1501.
(12) Brongersma, M. L.; Hartman, J.; Atwater, H. A. *Phys. Rev. B* **2000**, *62*, R16356.
(13) Gramotnev, D. K. *J. Appl. Phys.* **2005**, *98*, 104302.
(14) Gramotnev, D. K.; Vernon, K. C. *Appl. Phys. B* **2007**, *86*, 7.
(15) Wang, H.; Levin, C. S.; Halas, N. J. *J. Am. Chem. Soc.* **2005**, *127*, 14992.
(16) Kneipp, K.; Wang, Y.; Kneipp, H.; Perelman, L. T.; Itzkan, I.; Dasari, R. R.; Feld, M. S. *Phys. Rev. Lett.* **1997**, *78*, 1667.
(17) Pettinger, B.; Ren, B.; Picardi, G.; Schuster, R.; Ertl, G. *Phys. Rev. Lett.* **2004**, *92*, 096101.
(18) Ichimura, T.; Hayazawa, N.; Hashimoto, M.; Inouye, Y.; Kawata, S. *Phys. Rev. Lett.* **2004**, *92*, 220801.
(19) Nie, S. M.; Emory, S. R. *Science* **1997**, *275*, 1102.
(20) Babadjanyan, A. J.; Margaryan, N. L.; Nerkararyan, K. V. *J. Appl. Phys.* **2000**, *87*, 8.
(21) Anderson, N.; Bouhelier, A.; Novotny, L. *J. Opt. A* **2006**, *8*, S227.
(22) Li, K.; Stockman, M. I.; Bergman, D. *J. Phys. Rev. Lett.* **2003**, *91*, 227402.
(23) Nerkararyan, K. V. *Phys. Lett. A* **1997**, *237*, 103.
(24) Liu, Z.; Steele, J. M.; Srituravanich, W.; Pikus, Y.; Sun, C.; Zhang, X. *Nano Lett.* **2005**, *5*, 1726.
(25) Su, K.; Durant, S.; Steele, J. M.; Xiong, Y.; Sun, C.; Zhang, X. *J. Phys. Chem. B* **2006**, *110*, 3964.
(26) Prodan, E.; Radloff, C.; Halas, N. J.; Nordlander, P. *Science* **2003**, *302*, 419.
(27) Lide, D. R., Ed. *CRC Handbook of Chemistry and Physics*, Internet Version 2007, 87th Edition; Taylor and Francis: Boca Raton, FL, 2007. http://www.hbcpnetbase.com.

NL062911Y